Raman intensities and interference effects for thin films adsorbed on metals

Joel W. Ager III, D. Kirk Veirs, and Gerd M. Rosenblatt

Citation: The Journal of Chemical Physics **92**, 2067 (1990); doi: 10.1063/1.458040
View online: http://dx.doi.org/10.1063/1.458040
View Table of Contents: http://scitation.aip.org/content/aip/journal/jcp/92/3?ver=pdfcov
Published by the AIP Publishing

Raman intensities and interference effects for thin films adsorbed on metals

Joel W. Ager III, D. Kirk Veirs, and Gerd M. Rosenblatt
Center for Advanced Materials, Materials and Chemical Sciences Division, Lawrence Berkeley Laboratory, Berkeley, California 94720

(Received 18 September; accepted 26 October 1989)

Large oscillations in the vibrational Raman intensity have been observed for thin films adsorbed on a metal substrate as a function of film thickness. The systems studied, N_2 and O_2 physisorbed on Ag(111) at 14 ± 1 K, have previously been shown to be unenhanced, i.e., the observations are not caused by the surface enhanced Raman (SERS) effect. The observed oscillations are due to multiple beam interference caused by reflections at the film boundaries of the incident laser light and, to a lesser extent, the Raman scattered light. We extend the two-dimensional theoretical development of Moscovits and co-workers for Raman scattering in thin films to include more general three-dimensional experimental geometries. We derive expressions for the total intensity as a function of film thickness, incident laser polarization and angle, and scattered light polarization and angle. The resultant expressions are applicable to Raman scattering from any dielectric thin film adsorbed on a substrate with known optical parameters. Although complicated, the general expressions have been numerically evaluated for our experimental conditions using a commercial mathematical package on a personal computer. The calculated Raman intensities are in excellent agreement with the experimental results. The observed period of the intensity oscillation relates the film thickness to the exposure allowing the sticking probabilities to be determined. The sticking probabilities of N_2 on N_2 and O_2 on O_2 at 14 ± 1 K are 0.84 ± 0.2 and 0.82 ± 0.2, respectively.

I. INTRODUCTION

The existence of multiple beam interference effects in Raman scattering from thin films was first observed by DiLella *et al.*[1] in a surface enhanced Raman study of CO adsorbed on Ag. Nemanich and co-workers found that the Raman signal from thin layers of tellurium[2] and Pd_2Si[3] was enhanced by constructive interference due to the imposition of a dielectric layer between the scattering layer and the underlying reflective aluminum substrate. Hayashi and Samejima[4] found that the SERS intensity from a thin layer of copper phythalocyanine on Ag and Si was nonlinear with increasing layer thickness up to 80 nm and began to show oscillations. They attributed this behavior to multiple interference in the film. Ohsawa *et al.*[5] found that the angular distribution of Raman scattering from 7,7', 8,8'-tetracyanoquinodimethane on aluminum was a function of layer thickness. More recently, McCarty[6] has observed small oscillations in the Raman intensity of a Na_2SO_4 layer on a Pt/10%Rh alloy as a function of layer thickness for coverages up to 800 nm.

We distinguish two thickness regimes in the Raman study of thin films: layer thicknesses much smaller than the wavelength of the laser light and layer thicknesses from about one-quarter of the laser wavelength to many wavelengths. In the first case, interference effects arise from a single reflection from the substrate. This case was first discussed by Greenler and Slager.[7] Moskovits[8] used similar geometrical optics arguments to derive surface selection rules for Raman scattering from monolayer coverages on metal surfaces. Surface selection rules for very thin films were also derived using an image dipole method by Hallmark and Campion.[9] Recently, Crawford[10] has derived general E field equations for an emitting dipole in a film of arbitrary thickness above a metal substrate and has proposed somewhat different selection rules.

In the case of a thicker film, interference can also arise from multiple reflections between the film/metal and film/enviroment interfaces. The intensity of light within a thin film on a reflective surface is a variation on the standard optics problem of plane parallel plates and has been treated by Johnson and Peterson.[11] Hansen[12] has solved the E field equations for the general n layer case. DiLella *et al.*[1] have derived equations for Raman scattering in two dimensions from a thin film on a metal substrate and have discussed the angular dependences of laser excitation and scattered light detection. Ohsawa *et al.*[5] have derived similar equations for more general experimental geometries. Hayashi and Samejima[4] have shown that the Raman intensity as a function of layer thickness displays oscillations due to multiple interference by integrating the equations of DiLella *et al.*[1] over the thickness of the film. However, they restricted their analysis to p-polarized light.

We have observed large oscillations in the vibrational Raman intensity as a function of coverage from physisorbed films of N_2 and O_2 on Ag(111) at cryogenic temperatures for both s- and p-polarized laser light. We show that this effect is due to multiple beam interference effects involving multiple reflections between the film/metal and film/vacuum interfaces. We are not observing SERS but ordinary Raman scattering. We present experimental observations of interference effects in the Raman scattering intensity from thin films over a range of coverages from approximately ten to several hundred nm. We extend the theory to general inci-

 0021-9606/90/032067-10$03.00

dent laser and collection geometries and apply it to our experimental results.

II. EXPERIMENTAL METHOD

The experimental apparatus, which was designed to allow observation of unenhanced Raman scattering from submonolayer coverages of physisorbed systems, has been described in detail previously[13] so only a brief description will be given here. The ultrahigh vacuum chamber contains Auger and LEED surface characterization, Ar ion bombardment, and electron beam heating for sample cleaning and annealing, cryogenic cooling, and a wide range of sample manipulation. The Raman spectroscopy instrument consists of an Ar ion laser operating at 488 nm, beam shaping and collection optics, single monochromator, 2D imaging PMT detector, and computer data-acquisition electronics. A telescope was added to the optical system to improve beam quality and to expand the beam by a factor of six to create a tighter focus at the sample. The beam was focused onto the sample by a 300 mm focal length lens. The laser power entering the UHV chamber was 100 mW. The scattered light was collected by a 50 mm focal length $f/1$ lens and imaged by a 350 mm achromat through a bandpass filter and Glan–Thompson polarizer onto the entrance slit of the monochromator. Only a small fraction of the slit height is filled with scattered light with these optics and thus only about 10 vertical pixels on the 2D detector are summed to yield intensity in a given wavelength channel. With the 2400 groove/mm grating used here, the dispersion is 0.4 cm^{-1} pixel.

The geometry of the optical system is of particular importance to the magnitude of the observed interference effects and will be described in detail here. The laser angle of incidence was 70° from the Ag surface normal. The center of the collection lens was oriented at 36° to the surface normal in a plane perpendicular to the laser plane of incidence. The polarization convention for both the incident laser light and the scattered Raman light is that the E vector of p-polarized light is in the plane containing the propagation vector and the surface normal and the E vector of s-polarized light is normal to this plane. With this convention, when the detection plane is perpendicular to the laser plane of incidence as in the present experiments, the plane containing the E vector and propagation vector of p-polarized incident light is always perpendicular to the plane containing the E vector and propagation vector of p-polarized scattered light.

The sensitivity is limited by the background signal, which is related to sample cleanliness and surface morphology.[14] The Ag substrate was cleaned by several cycles of Ar ion bombardment and annealing to reduce the background signal observed at the vibrational Raman shift of the adsorbed gas. With the cleanest samples, the background count from the sample was constant across the N_2 and O_2 Raman shift regions at about 10 counts s^{-1} $channel^{-1}$. This is about a factor of 10 too high to observe submonolayer coverages but sufficiently low for the thicker films studied here. The smallest observed exposure in this work was 50 L of N_2 at 100 s integration time.

Films were grown by physisorption from bulk gas introduced through a leak valve to a known pressure measured with an ion gauge. The residual gas analyzer in the UHV chamber provided a convenient mass spectrometric check of gas purity (99.9995% for N_2 and 99.996% for O_2) and for the manufacturer's ion gauge calibration (readings from the ion gauge and the RGA mass spectrometer agreed to within 10%). The Raman intensity as a function of gas exposure was measured by exposing the sample for 100 s at $2–3\times10^{-6}$ Torr with all pumps off, pumping down to 1×10^{-9} Torr, collecting the Raman spectrum for 100 s, and repeating the procedure, thus building up coverages of several 1000 L in steps of a few 100 L. A typical Raman spectrum of 800 L of N_2 is shown in Fig. 1. Note the observation of $^{14}N–^{15}N$ in natural abundance (0.37%) at 2290 cm^{-1}. Intensity calculations and fits were carried out using the peak height minus the background as the measured of signal intensity; essentially the same results are obtained by using the integrated peak areas.

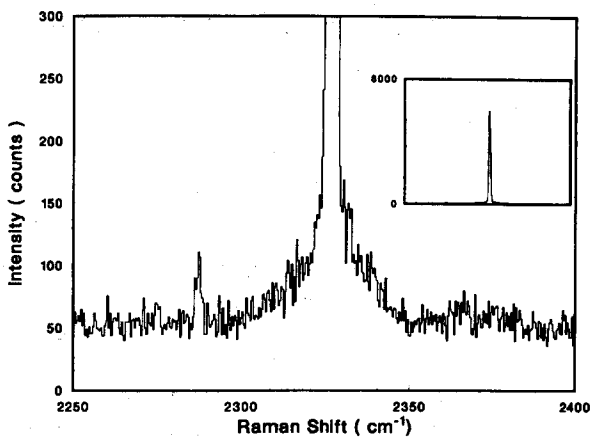

FIG. 1. Raman spectrum of N_2 physisorbed on Ag(111) at 14 K: 800 L exposure, s-polarized incident light, p-polarized collected light, 100 mW laser power, 100 s collection time. The insert has the same x axis scale and shows the full height of the $^{14}N_2$ peak. Note the observation of the $^{15}N–^{14}N$ line in 0.37% natural abundance at 2290 cm^{-1}.

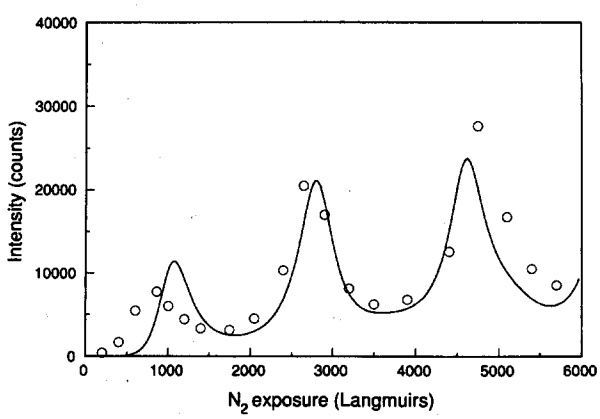

FIG. 2. The Raman intensity at 2325 cm^{-1} of N_2 physisorbed on Ag(111) at 14 K as a function of N_2 exposure. Experimental conditions: s-polarized incident light at 70°, p-polarized collected light at 36°, 100 mW laser power, 100 s collection time. The experimental data are indicated by the circles; the line is the theoretical prediction from Eq. (9d). The only adjustable parameters in the theoretical line are the instrument response and the sticking coefficients of N_2 on N_2.

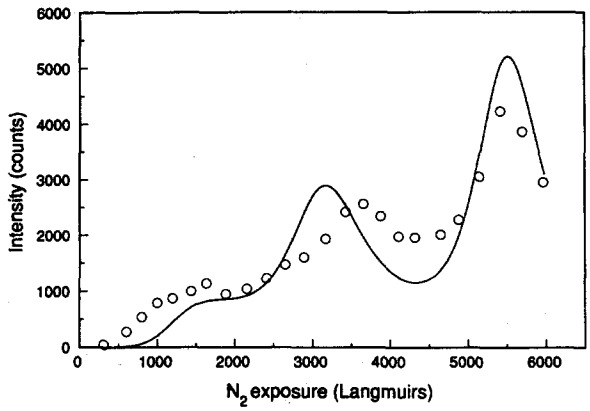

FIG. 3. The Raman intensity at 2325 cm^{-1} of N_2 physisorbed on Ag(111) at 14 K as a function of N_2 exposure. Experimental conditions: *p*-polarized incident light at 70°, *s*-polarized collected light at 36°, 100 mW laser power, 100 s collection time. The experimental data are indicated by the circles; the line is the theoretical prediction from Eq. (9d). The only adjustable parameters in the theoretical line are the instrument response and the sticking coefficient of N_2 on N_2.

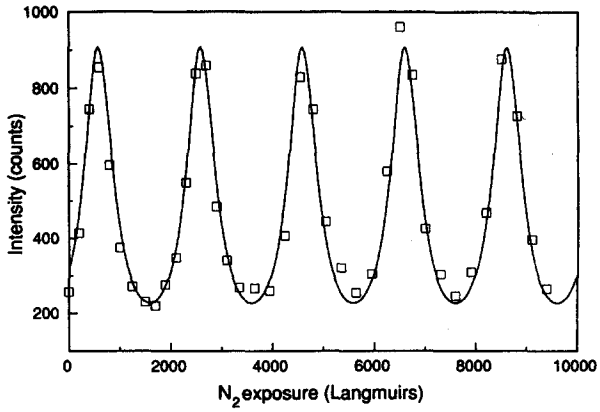

FIG. 5. The Raman intensity at 1550 cm^{-1} from a 300 L exposure of O_2 on Ag(111) at 14 K as a function of additional N_2 exposure. Experimental conditions: *s*-polarized incident light, *p*-polarized collected light. The experimental data are indicated by the squares; the line is a 4 parameter fit to Eq. (15) with a constant l in the numerator. The oscillations arise from constructive and destructive interference of the incident laser light.

III. EXPERIMENTAL RESULTS

We have observed previously that the Raman intensity from thin films of N_2 on Ag (111) increases linearly with exposure for small coverages[14]; this is clearly not the case for the larger coverages in this work. The points in Fig. 2 show the measured N_2 vibrational Raman signal as a function of N_2 exposure for *s*-polarized laser light and *p*-polarized collection. The points in Fig. 3 show the measured N_2 Raman intensity for *p*-polarized laser light and *s*-polarized collection. The points in Fig. 4 show the measured O_2 vibrational Raman intensity for *s*-polarized laser light and *p*-polarized collection as a function of O_2 exposure. The intensity oscillations due to the interferences of the laser and scattered light are easily observed in Figs. 2–4. In the experiment shown in Fig. 5, we exposed the sample first to 300 L O_2 and observed the O_2 vibrational Raman signal at 1550 cm^{-1}. The sample was then exposed to increasing coverages of N_2 and etalon-like oscillations in the O_2 Raman signal from the constant thickness of 300 L of O_2 were observed as the N_2 exposure was increased. The solid lines in Figs. 2–5 are fits to the data using theoretical expressions developed below.

IV. THEORY

The derivation of the amplitudes of the E fields due to the laser and scattered light within a uniform flat film has been treated previously in two dimensions,[1,4–6,11,12] and each author has used a different coordinate system and choice of initial phase. In our development, we use the sign and phase conventions suggested as standards for ellipsometry by Muller.[15]

Figure 6 shows the pertinent paths within a film for the incident laser light and scattered Raman light. As shown in Fig. 6(a), the laser is incident from the positive y direction, the electric field vector of *s*-polarized incident light is paral-

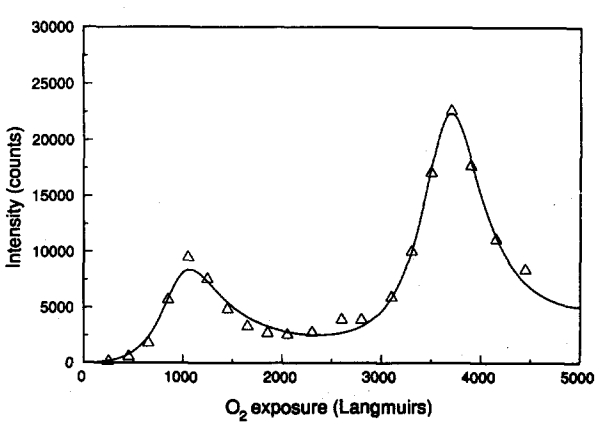

FIG. 4. The Raman intensity at 1550 cm^{-1} of O_2 physisorbed on Ag(111) at 14 K as a function of exposure. Experimental conditions: *s*-polarized incident light, *p*-polarized collected light. The experimental data are indicated by the triangles; the line is a 5 parameter fit to Eq. (14) considering only the interference of the incident light.

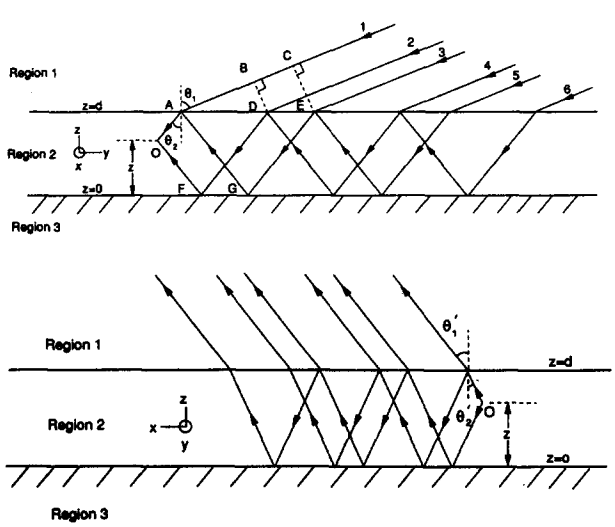

FIG. 6. Optical paths in a thin film: (a) incident light; (b) scattered light.

lel to the x axis, the electric vector of p-polarized incident light is in the yz plane, and $z = 0$ at the surface of the metal. In our experiments region 1 is vacuum, region 2 is solid N_2 or O_2, and region 3 is Ag; however, the derivation is general. We consider a plane wave from the laser that is incident on the film surface at an angle θ_1 from the surface normal. We now construct the complex amplitude of the E field at point **O**, a distance z above the surface of the metal in a film of thickness d. It is convenient to consider the rays coming from directions **AO** and **FO** separately. We set the zero of phase to be at **O** and calculate the optical paths. Our phase convention differs from that of DiLella *et al.*,[1] who set the zero of phase at **A**; the present choice results in equivalent, but simpler looking, formulas. Of course, all absolute phase information is lost when the E fields are squared to compute the intensities. The amplitude of the total E field in direction **AO** due to the laser is constructed from the sum of rays, 1, 3, 5, etc. The optical path difference between rays 1 and 3 is **EG** + **GA** − **AC**, leading to a phase difference of δ,

$$\delta = \frac{4\pi n_2 d \cos\theta_2}{\lambda}. \tag{1}$$

where λ is the laser wavelength, n is the index of refraction, θ_2 is obtained from the laser angle of incidence θ_1 using Snell's law, $n_1 \sin\theta_1 = n_2 \sin\theta_2$, and the subscripts on n and other variables refer to the regions. We have assumed $n_1 = 1$. The optical path difference between rays 3 and 5, etc. is also δ and we construct a series sum,

$$\mathbf{E}_d = t_{12}\mathbf{E}_0[1 + r_{23}r_{21}e^{i\delta} + r_{23}^2\, r_{21}^2\, e^{i2\delta} + \cdots]$$

which converges to

$$\mathbf{E}_d = \frac{t_{12}\mathbf{E}_0}{1 - r_{21}r_{23}e^{i\delta}}, \tag{2}$$

where $\mathbf{E}_0$ is the amplitude of the incident laser field, and r_{21}, r_{23}, and t_{12} are reflection and transmission coefficients for the subscripted interfaces calculated from the complex Fresnel equations.[16] The symbol r_{12} means that the light is traveling in region 2 and is reflected at the 2–1 interface; the symbol t_{12} means that the light passes though the 1–2 interface from region 1 into region 2. For metallic substrate, r_{23} is a complex number (because n_3 is a complex number) and contains the phase change for reflection. Now we consider the rays headed in direction **FO**. The optical path difference between rays 1 and 2 is **FO** + **DF** − **AB** − **AO** leading to a phase difference of

$$\delta_z = \frac{4\pi n_2 z \cos\theta_2}{\lambda}. \tag{3}$$

Subsequent rays (2, 4, 6, etc.) have a path difference of δ as before and the sum

$$\mathbf{E}_r = \mathbf{E}_0 t_{12} r_{23} e^{i\delta_z}[1 + r_{21}r_{23}e^{i\delta} + r_{21}^2\, r_{23}^2\, e^{i2\delta} + \cdots]$$

converges to

$$\mathbf{E}_r = \frac{\mathbf{E}_0 t_{12} r_{23} e^{i\delta_z}}{1 - r_{21}r_{23}e^{i\delta}}. \tag{4}$$

The total amplitude at point **O** is then $\mathbf{E}_d + \mathbf{F}_r$

$$\mathbf{E}_{\text{total}} = \frac{1 + r_{23}\, e^{i\delta_z}}{1 - r_{21}r_{23}\, e^{i\delta}}\, t_{12}\mathbf{E}_0. \tag{5}$$

Incident light that is p-polarized has a component in the surface plane and a component normal to the surface plane, whereas s-polarized incident light only has a component in the surface plane. We indicate this by resolving Eq. (5) into its components:

$$E_x = \frac{1 + r_{23}^s\, e^{i\delta_z}}{1 - r_{21}^s\, r_{23}^s e^{i\delta}}\, t_{12}^s\, \mathbf{E}_0^s \tag{6a}$$

$$E_y = \frac{-1 + r_{23}^p\, e^{i\delta_z}}{1 - r_{21}^p\, r_{23}^p e^{i\delta}}\, t_{12}^p\, \mathbf{E}_0^p \cos\theta_2 \tag{6b}$$

$$E_z = \frac{1 + r_{23}^p\, e^{i\delta_z}}{1 - r_{21}^p\, r_{23}^p e^{i\delta}}\, t_{12}^p\, \mathbf{E}_0^p \sin\theta_2 \tag{6c}$$

where $\mathbf{E}_0^s$ and $\mathbf{E}_0^p$ are the components of the incident E field (i.e., the laser polarization) and the superscripts on $\mathbf{E}_0$ and the Fresnel coefficients refer to the laser polarizations. The Fresnel reflection and transmission coefficients in the above equations depend strongly upon polarization and angle and changes in the values of these variables affect the behavior of the Raman intensity as a function of exposure. Equations (1)–(6) are equivalent to those derived by Johnson and Peterson[11] and DiLella *et al.*[1] except for unimportant phase differences due to different choices of the zero of absolute phase.

The induced dipole $\mathbf{p}$ is coupled to the E field of the laser through the derived polarizability tensor α'[17]:

$$\mathbf{p} = \alpha'\mathbf{E}. \tag{7}$$

The construction of the derived polarizability tensor for our experimental conditions is discussed in Sec. V.

The Cartesian components of the E field of the Raman scattered light are proportional to the components of the induced dipole. In a nominally 90° scattering geometry, the scattered light that is detected [Fig. 6(b)] propagates in the positive x direction and undergoes interference from multiple reflections in the same way as the laser light. We note here that the derivation can be extended to any angle between the incident and scattered light plane by rotating $\mathbf{p}$ with a rotation matrix.[18] The derivation of the scattered light electric field due to multiple interference is analogous to that for the incident light and will be stated here without proof; the primes on all the variables signify that they are for the scattered light. As before, θ_2' is computed from the laboratory angle θ_1' by Snell's law. For our experimental geometry, the E vector of the scattered s-polarized light is along the y axis and the E vector of the scattered p-polarized light is in the xz plane.

$$E_x' = \frac{-1 + r_{23}'^p\, e^{i\delta_z'}}{1 - r_{21}'^p\, r_{23}'^p\, e^{i\delta'}}\, t'^p_{12} p_x \cos\theta_2', \tag{8a}$$

$$E_y' = \frac{1 + r_{23}'^s\, e^{i\delta_z'}}{1 - r_{21}'^s\, r_{23}'^s\, e^{i\delta'}}\, t'^s_{21}\, p_y, \tag{8b}$$

$$E_z' = \frac{1 + r_{23}'^p\, e^{i\delta_z'}}{1 - r_{21}'^p\, r_{23}'^p\, e^{i\delta'}}\, t'^p_{12} p_z \sin\theta_2', \tag{8c}$$

where r's and t's are reflection and transmission coefficients for the scattered light at the subscript interfaces calculated using θ_1' and θ_2' and the indices of refraction of the three regions at the scattered light wavelength.[16] Again, r_{23}' is complex for a metallic substrate.

The total intensity of Raman scattered light from a film

is found by integrating appropriate combinations of Eqs. (8a)–(8c) over the thickness of the film. Since we are interested in relative intensities only, terms referring to the absolute Raman cross section, laser power, collection solid angle, and instrument response are not included. We identify four cases: *ss*, *pp*, *sp*, and *ps*, where the letters stand for the polarization of the laser and scattered light, respectively, and construct the total scattered intensities:

$$I^{ss}(d) = \int_0^d |E'_y|^2 dz, \quad E_0^s = E_0, \quad E_0^p = 0, \tag{9a}$$

$$I^{ps}(d) = \int_0^d |E'_y|^2 dz, \quad E_0^s = 0, \quad E_0^p = E_0, \tag{9b}$$

$$I^{pp}(d) = \int_0^d (|E'_x|^2 + |E'_z|^2) dz, \quad E_0^s = 0, \quad E_0^p = E_0, \tag{9c}$$

$$I^{sp}(d) = \int_0^d (|E'_x|^2 + |E'_z|^2) dz, \quad E_0^s = E_0, \quad E_0^p = 0. \tag{9d}$$

Recall that E_0 is the amplitude of the incident laser electric field. The intensities are functions of the layer thickness d, and the incident and collection angles θ_1 and θ'_1. Similar equations for scattered light collection in the laser plane of incidence (2D experimental geometry) can be found in DiLella *et al.*[1] We note here that, in principle, the derivation is more general than we have indicated and can be extended to Rayleigh scattering by using the polarizability tensor (instead of the derived polarizability tensor) and setting $\lambda = \lambda'$ and to fluorescence by replacing Eq. (7) with the dipole moment operator. Equations (9a)–(9d) can be numerically integrated to yield intensities for a particular case and this will be done in Sec. V. However, we will also show that under certain conditions the intensiy variation as a function of d can be modeled by analytical forms that have a simple physical interpretation.

V. DISCUSSION

Equations (9d) and (9b) correspond to our experimental measurements for N_2 on Ag(111) with incident *s*- and collected *p*-polarized light (Fig. 2) and incident *p*- and collected *s*-polarized light (Fig. 3). The input parameters for these equations are the derived polarizability tensor and the reflection and transmission coefficients. The reflection and transmission coefficients are calculated[16] from the known experimental values of θ_1 and θ'_1 and the refractive indices of regions 1, 2, and 3. We use $n_1 = 1$ for the vacuum and $n_3 = 0.177 - 3.638i$ for Ag.[19] We calculate $n_2 = 1.255$ for solid N_2 and 1.308 for solid O_2 at 15 K from the Lorentz-Lorenz equation [20] using polarizabilities for N_2 and O_2 of 1.7403×10^{-24} cm^{-3} and 1.5812×10^{-24} cm^{-3}, respectively [21]. We use densities for solid α-N_2 and α-O_2 of 1.026 and 1.530 g cm^{-3}, respectively, at 14 K.[22] The laser wavelength, λ, is 488 nm and the scattered wavelength, λ', is 550.3 nm for N_2 and 527.9 nm for O_2. We use a molecule fixed derived polarizability tensor for N_2 of $\alpha'_{xx} = \alpha'_{yy} = 3.89$ and $\alpha'_{zz} = 10.61$ in atomic units.[23] We assume that the molecules are randomly oriented and average over all angles[24] to obtain the space fixed derived polarizability tensor used in the calculations.

We have numerically integrated Eqs. (9a)–(9d) for α-N_2 on Ag and our experimental geometry ($\theta_1 = 70°$ and $\theta'_1 = 36°$) using at AT class personal computer and a commercial mathematical software package.[25] The results are shown in Figs. 2 and 3 together with the corresponding experimental data. For thick films $I^{ss}(d)$ and $I^{pp}(d)$ are more than an order of magnitude smaller than $I^{sp}(d)$ and $I^{ps}(d)$. Since the theory predicts only relative intensities the theoretical results were adjusted to match the observed data by scaling the x and y coordinates. However, there are no other adjustable parameters in the model to change, for example, the shapes of the curves. In light of this, the correspondence of the theory with the experimental data appears good, although the theory predicts somewhat larger oscillation amplitudes for the *ps* experiment (Fig. 3) than are observed.

In general, the interferences of both the laser and the scattered light affect the magnitude of the Raman signal from a thin film. However, it is useful to have less complex analytical formulas than Eq. (9) to model the Raman intensity as a function of film thickness at a particular polarization and experimental geometry. The multiple interference effect that causes the large observed oscillations in the Raman intensity as a function of film thickness is dependent on the values of the reflection coefficients, r_{21} and r'_{21}, which increase significantly as one moves towards glancing angles. Thus, when the incident laser angle θ_1 is large compared to the collection angle θ'_1, the Raman intensity as a function of film thickness is largely determined by multiple interference of the laser light. Under these conditions, by neglecting the interference of the scattered light, one can obtain simple analytical expressions which are in good agreement with the data and with the general solutions given in Eqs. (9a)–(9d).

We begin with Eqs. (6a)–(6c) which express the magnitude of the incident light E field as a function of position within the film. We now explicitly acknowledge r_{23} to be a complex number and introduce two additional phases, $\phi^s = \arg(r^s_{23})$ and $\phi^p = \arg(r^p_{23})$, the phase changes for s and p light the metal surface, and note the identity $\delta_z = \delta z/d$. We recall that r_{ij} and t_{ij} depend upon the angle of incidence.[16] The intensity due to interference of the incident light, as a function of position in the film, is

$$I_x(z) = |E_x|^2 = \frac{1 + |r^s_{23}|^2 + 2|r^s_{23}|\cos[(\delta z/d) + \phi^s]}{(1 - r^s_{21}|r^s_{23}|)^2\{1 + F_s \sin^2[(\delta + \phi^s)/2]\}} \times |t^s_{12}|^2 |E^s_0|^2, \tag{10a}$$

$$I_y(z) = |E_y|^2 = \frac{1 + |r^p_{23}|^2 - 2|r^p_{23}|\cos[(\delta z/d) + \phi^p]}{(1 - r^p_{21}|r^p_{23}|)^2\{1 + F_p \sin^2[(\delta + \phi^p)/2]\}} \times |t^p_{12}|^2 |E^p_0|^2 \cos^2\theta_2, \tag{10b}$$

$$I_z(z) = |E_z|^2$$
$$= \frac{1 + |r_{23}^p|^2 + 2|r_{23}^p|\cos[(\delta z/d) + \phi^p]}{(1 - r_{21}^p|r_{23}^p|)^2\{1 + F_p \sin^2[(\delta + \phi^p)/2]\}} \times |t_{12}^p|^2|E_0^p|^2 \sin^2\theta_2, \quad (10c)$$

where

$$F^s = \frac{4r_{21}^s|r_{23}^s|}{(1 - r_{21}^s|r_{23}^s|)^2} \quad (11a)$$

and

$$F^p = \frac{4r_{21}^p|r_{23}^p|}{(1 - r_{21}^p|r_{23}^p|)^2}. \quad (11b)$$

These equations are reminiscent of the Airy formula for interference in an etalon, where F is the coefficient of finesse[26] and serves as a measure of the multiple interference effect.[27]

To obtain the total intensity within the film arising from the illuminating laser, we integrate Eqs. (10a)–(10c) over the film thickness for s and p laser polarization:

$$I^s(d) = \int_0^d I_x(z)dz$$
$$= \frac{1 + |r_{23}^s|^2 + 2|r_{23}^s|\{[\sin(\delta + \phi^s) - \sin\phi^s]/\delta\}}{(1 - r_{21}^s|r_{23}^s|)^2\{1 + F_s \sin^2[(\delta + \phi^s)/2]\}} \times |t_{12}^s|^2|E_0^s|^2 d, \quad (12a)$$

and

$$I^p(d) = \int_0^d I_y(z) + I_z dz$$
$$= \frac{1 + |r_{23}^p|^2 - 2|r_{23}^p|\cos 2\theta_2\{[\sin(\delta + \phi^p) - \sin\phi^p]/\delta\}}{(1 - r_{21}^p|r_{23}^p|)^2\{1 + F^p \sin^2[(\delta + \phi^p)/2]\}} \times |t_{12}^p|^2|E_0^p|^2 d. \quad (12b)$$

When multiple interference of the Raman scattered light is negligible, the Raman intensity is directly proportional to the total illumination intensity in the scattering film. Under these conditions, Eq. (12a) allows one to compute the relative variation with film thickness d of the Raman intensity produced by s-polarized light, for a given angle of incidence θ_1 and at a fixed angle of collection θ_1'. Recall, from Eq. (1), that the phase difference δ varies linearly with d. Similarly, Eq. (12b) allows one to compute the relative variation with film thickness of the Raman intensity produced by p-polarized light, for a given angle of incidence, with a fixed collection geometry. However, because the Raman scattering produced by s- and p-polarized laser light changes, and changes differently, with collection angle and polarization analysis, Eqs. (12a) and (12b) cannot be compared to yield the relative intensities of Raman scattering produced by s- and p-polarized light, except in the special (and not experimentally realizable) case where all the Raman scattered light emitted into the 2π solid-angle hemisphere is collected. If one is interested in comparing the relative Raman intensities produced by s- and p-polarized incident light, Eq. (9) must be used.

The total laser intensity within the film calculated from Eq. (12) shows oscillations as a function of film thickness d.

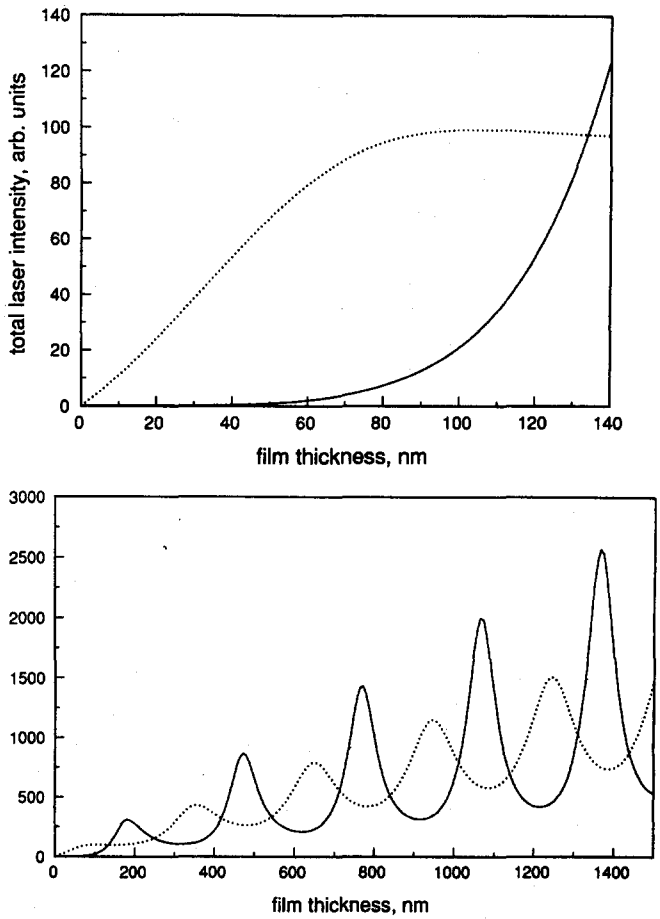

FIG. 7. Illumination intensity within an N_2 film on Ag integrated over the thickness of the film from Eq. (12) with $n_2 = 1.495$ (α-N_2) and $\theta_1 = 70°$: (a) for small coverages; (b) for larger coverages. The solid line is for s-polarized incident light and the dotted line is for p-polarized incident light. Under appropriate conditions (see text) the illumination intensity can be used to model the Raman intensity at a given geometry as a function of film thickness.

This is shown in Fig. 7 for α-N_2 on Ag and our experimental geometry ($\theta_1 = 70°$). We will discuss the results in the context of the two regimes mentioned in the Introduction: films whose thicknesses are much smaller than the wavelength of light and thicker films. We can model very thin films by ignoring multiple interference caused by internal reflections at the film/vacuum interface. We set $r_{21} = 0$, which causes the denominators of Eqs. (12a) and (12b) to become one. For coverages from one monolayer to a few monolayers, the phase change for one traversal of the film can be neglected, so $\delta \approx 0$, leading to further simplifications. The result is a constant illumination intensity across the film and integrated intensities that are linear in d:

$$I^s(d) = \left(1 + |r_{23}^s|^2 + 2|r_{23}^s|\cos\phi^s\right)|t_{12}^s|^2|E_0^s|^2 d, \quad (13a)$$

$$I^p(d) = \left(1 + |r_{23}^p|^2 - 2|r_{23}^p|\cos 2\theta_2 \cos\phi^p\right) \times |t_{12}^p|^2|E_0^p|^2 d. \quad (13b)$$

These equations are similar to those derived by Moskovits[8] and Greenler and Slager[7] and produce the linear part of the

curves shown in Fig. 7(a) up to a film thickness of about 40 nm. For a very thin film on a metal $\phi^s \simeq \pi$ and $I^s(d)$, the intensity resulting from *s*-polarized incident light, is small for all incident angles due to destructive interference at the surface. For *p*-polarized incident light, the competing $\cos 2\theta_2$ and $\cos \delta^p$ terms lead to a more complicated behavior for $I^p(d)$ as a function of θ_2; this has been discussed by Moskovits[8] and by Greenler and Slager.[7] The overall conclusion is that the largest total illumination intensities for sub- and near-monolayer coverages are expected for *p*-polarized laser light incident at angles around 70°.

For thicker films multiple interference is important; Eqs. (12a) and (12b) must be used to calculate the laser intensity in the film, and (in contrast to the monolayer case) *s*-polarized laser light yields the largest total illumination intensities as shown in Fig. 7(b). Since $r^s_{21} > r^p_{21}$ for all angles and since the coefficient of finesse F is a strongly increasing function of r_{21}, the multiple interference effect is always greater for *s*-polarized light. The intensities as a function of d for the two polarizations are also approximately π out of phase, corresponding to the relative phase difference for the reflection of *s* and *p* light at a metal/dielectric interface.[28] The separation between maxima of intensity is $\lambda/(2n_2 \cos\theta_2)$ as can be seen in Fig. 7(b).

Equations similar to (12a) and (12b) with r, t, and θ replaced by primed quantities can be derived by considering the interference of the scattered light only. These would describe the scattered intensity for, for example, small incident laser angles and large collection angles. The values of F and F' calculated in this way, by considering the interferences of the laser and scattered light separately, depend upon r_{21} and r'_{21} and, thus, upon the incident laser and scattered light collection angles. By adjusting these angles, the coefficients of finesse can be controlled by the experimenter so that multiple interference of either the laser or the scattered light dominates. For example, to optimize the geometry to favor interference of the incident light, one would use *s*-polarized incident laser light at a high (near glancing) angle and detect *p*-polarized light at the Brewster angle ($\theta'_1 = 54°$ for α-N_2).

Since in our experiments the incident laser angle θ_1 is considerably larger than the collection angle θ'_1 (70° vs 38°), modeling the variation of Raman intensity as a function of d by neglecting interference of the scattered light is a good approximation. The relative importance of the interferences of the laser and the scattered light can be compared by computing the coefficients of finesse (which are related to the amplitudes of the oscillations) from Eq. (11) and its primed analog for laser only and scattered light only interference. For *s*-polarized laser light and *p*-polarized collection $F = 4.50$ and $F' = -0.209$, respectively. For *p*-polarized laser light and *s*-polarized collection $F = 1.29$ and $F' = 0.855$. In both cases the coefficients of finesse and thus the multiple interference effect is larger for the laser light, although the difference is less pronounced for the *ps* experiment.

Since the intensity pattern as a function of d in our experiments is largely determined by the interference of the incident light, Eqs. (12a) and (12b) can be used to measure the frequency and amplitude of the oscillations in the experimental data. Equation (12) can be rewritten in a general 5 parameter form:

$$I_{\rm exp}(l) = \frac{Ax + B\left[\sin(2\pi l/\Delta l_{\rm obs} + \delta_{\rm obs}) - \sin\delta_{\rm obs}\right]}{1 + F_{\rm obs}\left[\sin^2(\pi l/\Delta l_{\rm obs} + \delta_{\rm obs}/2)\right]}, \quad (14)$$

where l is the coverage in Langmuirs (measured experimentally), A is proportional to the sensitivity of the experiment, B is a measure of the two beam interference effect, $F_{\rm obs}$ is proportional to the modulation of the observed intensity, and $\Delta l_{\rm obs}$ is the spacing between maxima of intensity (in units of exposure, L). The value of $\Delta l_{\rm obs}$ can be used to relate the experimental exposure to the actual coverage. For large exposures, $Ax \gg B$, and one can set $B = 0$ and use a simpler 4 parameter asymptotic form:

$$I_{\rm exp}(l) = \frac{Ax}{1 + F_{\rm obs}\left[\sin^2(\pi l/\Delta l_{\rm obs} + \delta_{\rm obs}/2)\right]}. \quad (15)$$

We have performed nonlinear least squares fits to the experimental data in Figs. 1–4 using both Eqs. (14) and (15). The results are summarized in Table I; the fit is good for all the experiments. An example is given in Fig. 4 for O_2 on Ag(111) using Eq. (14). The experiment shown in Fig. 5 has a particularly simple physical interpretation. Since the

TABLE I. Results of fitting the experimental data to Eqs. (14) and (15). The value of $\Delta l_{\rm obs}$ is the observed spacing between intensity maxima in Langmuir units and $F_{\rm obs}$ is related to the amplitude of the oscillations.

Film	No. of data pts.	Laser polarization	Collection polarization	$\Delta l_{\rm obs}$[a] (L)	$F_{\rm obs}$[a]	Comment
N_2	20	*s*	*p*	2052(22)	3.25(0.32)	5 parameter fit, Eq. (14)
				2018(43)	3.21(0.49)	4 parameter fit, Eq. (15)
N_2	24	*p*	*s*	1947(40)	0.75(0.08)	5 parameter fit, Eq. (14)
				2022(41)	0.75(0.09)	4 parameter fit, Eq. (15)
300 L O_2 plus N_2[b]	38	*s*	*p*	2005(6)	2.99(0.20)	4 parameter fit to Eq. (15), see the text
O_2	20	*s*	*p*	2693(27)	4.83(0.35)	5 parameter fit, Eq. (14)
				2619(54)	4.66(0.53)	4 parameter fit, Eq. (15)

[a] Standard errors are in parentheses.
[b] The values of $\Delta l_{\rm obs}$ and $F_{\rm obs}$ are for the N_2 overlayer, see the text.

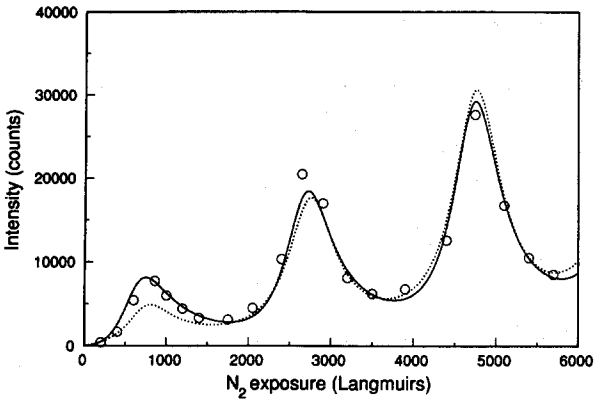

FIG. 8. Modeling the experimental data in Fig. 2, considering the interference of the incident laser light only and neglecting the interference of the scattered light. The solid line is a 5 parameter nonlinear least-squares fit to Eq. (14) and the dotted line is a 4 parameter fit to Eq. (15). The fits differ mainly in the vicinity of the first maximum.

amount of scattering material, the 300 L of O_2, remained constant as the thickness of the layer was increased, we fit the data to the average laser intensity in the film computed from Eq. (15) with a constant l in the numerator. The addition of N_2 layers modulates the total integrated laser intensity within the film. Since for our experimental geometry the interference of the laser is dominant, the Raman signal from O_2 is proportional to the laser intensity and exhibits etalon-like oscillations. Note that the scattering intensity from a constant amount of O_2 oscillates over a range of a factor of three.

Figure 8 compares the fits to Eq. (14) [5 parameters] and Eq. (15) [4 parameters] for the N_2 *sp* experiment from Fig. 2. After the first maximum the two fit curves are nearly identical, showing that multiple beam interference is more important than two beam interference for large coverages. For the same experimental data set, the values of F calculated from the 4 and 5 parameter fits to Eqs. (14) and (15) agree to within 3% (see Table I). The precision of the measurement of Δl_{obs} is very good; values for N_2 determined in three different experiments (the *sp* and *ps* experiments with pure N_2 and the N_2 on O_2 experiment) agree to within 1%. In order to compare quantitatively the magnitude of the observed and theoretical intensity oscillations, we used Eq. (14) to fit the theoretical predictions generated from Eqs. (9d) and (9b) for N_2 films. For the *sp* geometry the predicted F is 3.2, which is in good agreement with the observed value. For the *ps* geometry, the predicted F is 2.2, which is higher than the observed value.

The observed spacing between the intensity maxima Δl_{obs} (in exposure units), corresponds to a change in film thickness, Δd, which can be computed from the experimental geometry and film index of refraction. Thus, the sticking probability β can be calculated from the experimental exposure by equating Δl_{obs} with the film thickness that would be produced by an exposure of Δd_{obs}. As noted above, and as can be seen by comparing Eq. (1) for $\delta = n(2\pi)$ and $\delta = (n+1)2\pi$, the expected spacing between intensity maxima in thickness units is[29]

$$\Delta d = \lambda / 2n_2 \cos\theta_2. \tag{16}$$

We now calculate the film thickness corresponding to an experimental exposure. The number of molecules N condensed on area A of film in time t is

$$N/A = \beta J t, \tag{17}$$

where β is the sticking probability, J is the incident molecular flux density from the Hertz–Knudsen equation,

$$J = p/(2\pi m k T)^{1/2}, \tag{18}$$

m is the mass of a gaseous molecule, p and T are the pressure and temperature of the impinging gas, and k is the Boltzmann constant. The total mass of the film formed is $mN = \beta J t m A$ and thus the volume of the film is $V = \beta J t m A/\rho$ where ρ is the film density. The thickness of the film, $d = V/A$, is $d = \beta J t m/\rho$, and, introducing Eq. (18),

$$d = \frac{\beta p t}{\rho}\left(\frac{m}{2\pi k T}\right)^{1/2}. \tag{19}$$

Collecting constants, and expressing the exposure $l = pt$ in Langmuirs ($1\ \mathrm{L} = 10^{-6}$ Torr s), we can relate the experimental exposure to film thickness,

$$d = 0.583\left(\frac{\beta l}{\rho}\right)\left(\frac{m}{T}\right)^{1/2}, \tag{20}$$

with d in nm, ρ in g cm^{-3}, and m in amu.

The increase in film thickness that is produced by an exposure Δl_{obs} is

$$\Delta d = 0.583\beta\left(\frac{\Delta l_{obs}}{\rho}\right)\left(\frac{m}{T}\right)^{1/2}. \tag{21}$$

TABLE II. Experimental values of the sticking probability β for N_2 on N_2 and O_2 on O_2 at 14 ± 1 K. The values of β are calculated from Δl_{obs} in Table I using Eq. (22).

Experiment	β	Source of Δl_{obs}
N_2, *sp* polarization	0.83	5 parameter fit, Eq. (14), Fig. 8
	0.84	4 parameter fit, Eq. (15), Fig. 8
N_2, *ps* polarization	0.87	5 parameter fit, Eq. (14)
	0.84	4 parameter fit, Eq. (15)
300 L O_2 plus N_2, *sp* polarization[a]	0.85	4 parameter fit, Eq. (15) (see the text), Fig. 5
O_2, *sp* polarization	0.81	5 parameter fit, Eq. (14), Fig. 4
	0.83	4 parameter fit, Eq. (15)

[a] The sticking probability obtained in this experiment is for N_2 on N_2.

Equating Eqs. (16) and (21) and solving for β yields

$$\beta = 1.72\left(\frac{\lambda}{2n_2\cos\theta_2}\right)\left(\frac{\rho}{\Delta l_{\text{obs}}}\right)\left(\frac{T}{m}\right)^{1/2} \quad (22)$$

by which the sticking coefficient can be calculated from the experimental observations.

The values of the sticking probabilities for N_2 and O_2 calculated from Eq. (22) for the four experiments using both Eqs. (14) and (15) are listed in Table II. The scaling factors used to produce the lines in Figs. 2 and 3 can also be used to calculate the sticking probabilities. These values, 0.95 and 0.66 for the *sp* and *ps* experiment are in reasonable agreement with the values calculated from Eq. (22) for N_2 on N_2. The sticking probabilities of N_2 on N_2 and O_2 on O_2 at 14 ± 1 K are 0.84 ± 0.2 and 0.82 ± 0.2, respectively, where the uncertainties reflect our estimate of the random and systematic errors, mainly in the pressure at the Ag surface and the density of the film.

VI. CONCLUSIONS

We have observed oscillations in the vibrational Raman intensity from thin layers of N_2 and O_2 on Ag(111) at 14 ± 1 K as a function of film thickness. We use geometrical optics to derive general expressions for the Raman intensity as a function of film thickness which incorporate the interferences of both the incident excitation light and the Raman scattered light. These expressions are functions of the indices of refraction for the film and the metal, incident laser angle, scattered light collection angle, and derived polarizability tensor. The theoretical predictions are in good agreement with the experimental observations. In addition, the theory can also be used with only minor modifications to describe Rayleigh scattering and fluorescence from films on metals.

The theory shows that the oscillations in the Raman intensity are caused by interferences of the laser and scattered light within the film. The magnitude of the interference is strongly affected by the angle and polarization of the laser and scattered light. Furthermore, one can select experimental geometries with separate the effects of the incident laser light from those of the scattered light. In contrast to the monolayer case, for films thicker than a few hundred monolayers, maximum interference and maximum intensity occurs for *s*-polarized light at large angles and there is no multiple interference effect for *p*-polarized light at the film/vacuum Brewster angle. Thus, excitation by *s*-polarized laser light incident at a large angle and collection of *p*-polarized light near the Brewster angle ($\theta_1' = 56°$ for N_2) will result in intensity oscillations as a function of film thickness which are almost entirely due to interference of the laser light only. Under these conditions, the general expressions can be parametrized and the experimental data can be modeled by simple equations. Experimental exposure can then be related to coverage, allowing accurate measurements of film thickness and the calculation of sticking probabilities. The sticking probabilities of N_2 on N_2 and O_2 on O_2 at 14 ± 1 K are 0.84 ± 0.2 and 0.82 ± 0.2, respectively.

The maxima of the oscillations represent enhancement of the Raman signal above what one would expect from the number of scatters alone. The Raman intensity from a layer of O_2 as a function of the thickness of N_2 overlayers shows oscillations with a maximum enhancement in the signal of a factor of three. Thus, the addition of a carefully controlled thickness of an inert overlayer can be used to enhance the Raman signal from a very thin layer. Analytical expressions derived above can be used to optimize the physical properties of such an overlayer.

ACKNOWLEDGMENTS

This work was supported by the Director, Office of Energy Research, U. S. Department of Energy, at Lawrence Berkeley Laboratory under contract DE-AC-03-76SF-00098. We thank Rolf Muller for helpful discussions and Clint Cummins of TSP International for the use of statistical software.

[1] D. P. DiLella, A. Gohin, R. H. Lipson, P. McBreen, and M. Moskovits, J. Chem. Phys. **73**, 4282 (1980).
[2] G. A. N. Connell, R. J. Nemanich, and C. C. Tsai, Appl. Phys. Lett. **36**, 31 (1980).
[3] R. J. Nemanich, C. C. Tsai, M. J. Thompson, and T. W. Sigmon, J. Vac. Sci. Technol. **19**, 685 (1981).
[4] S. Hayashi and M. Samejima, Surf. Sci. **137**, 442 (1984).
[5] M. Ohsawa, W. Kusakari, and W. Suëtaka, Spectrochim. Acta Part A **36**, 389 (1980).
[6] K. F. McCarty, Appl. Opt. **26**, 4482 (1987).
[7] R. G. Greenler and T. L. Slager, Spectrochim. Acta Part A **29**, 193 (1969); R. G. Greenler, Surf. Sci. **69**, 647 (1977).
[8] M. Moskovits, J. Chem. Phys. **77**, 4408 (1982).
[9] V. M. Hallmark and A. Champion, J. Chem. Phys. **84**, 2933, 2942 (1986).
[10] O. H. Crawford, J. Chem. Phys. **89**, 6017 (1988).
[11] J. A. Johnson and D. W. Peterson, Surf. Sci. **16**, 217 (1969).
[12] W. N. Hansen, J. Opt. Sci. Am. **58**, 380 (1968).
[13] D. K. Veirs, V. K. F. Chia, and G. M. Rosenblatt, Appl. Opt. **26**, 3530 (1987); V. K. F. Chia, D. K. Veirs, and G. M. Rosenblatt, Rev. Sci. Instrum. **60**, 1161 (1989).
[14] D. K. Veirs, V. K. F. Chia, and G. M. Rosenblatt, Langmuir **5**, 633 (1989).
[15] R. H. Muller, Surf. Sci. **16**, 14 (1969).
[16] We use:

$$r_{ij}^s = \frac{n_i\cos\theta_i - n_j\cos\theta_j}{n_i\cos\theta_i + n_j\cos\theta_j},\quad r_{ij}^p = \frac{n_j\cos\theta_i - n_i\cos\theta_j}{n_j\cos\theta_i + n_i\cos\theta_j},$$

$$t_{ij}^s = \frac{2n_i\cos\theta_i}{n_i\cos\theta_i + n_j\cos\theta_j},\quad t_{ij}^p = \frac{2n_i\cos\theta_i}{n_j\cos\theta_i + n_i\cos\theta_j},$$

where the subscripts *i* and *j* refer to the regions. Muller, Ref. 15, discusses other phase conventions.
[17] D. A. Long, *Raman Spectroscopy* (McGraw–Hill, New York, 1977), p. 52.
[18] One substitutes $\mathbf{p}'$ for $\mathbf{p}$ where

$$\mathbf{p}' = \begin{pmatrix} \cos\phi & \sin\phi & 0 \\ -\sin\phi & \cos\phi & 0 \\ 0 & 0 & 1 \end{pmatrix}\mathbf{p},$$

and ϕ is the azimuthal angle, $\phi = 0$ for our experimental geometry. Rotation by $\pi/2$ produces the equations used by DiLella *et al.* for detecting the scattered light in the plane of the laser.
[19] F. A. Jenkins and H. E. White, *Fundamentals of Optics* (McGraw-Hill, New York, 1976), p. 538.
[20] M. Born and E. Wolf, *Principals of Optics* (Pergamon, New York, 1980), p. 87.
[21] T. M. Miller, in *Handbook of Chemistry and Physics*, 66th ed., edited by R. C. Weast (CRC, Boca Raton, 1985), pp. E65–74.
[22] J. Donahue, *The Structures of the Elements* (Wiley, New York, 1974), pp. 285 and 318.
[23] S. R. Langhoff, C. W. Bauschlicher, Jr., and D. P. Chong, J. Chem. Phys. **78**, 5287 (1983).

[24]E. B. Wilson, Jr., J. C. Decius, and D. C. Cross, *Molecular Vibrations* (Dover, New York, 1955), p. 46.
[25]We used MathCAD, version 2.5, for all our numerical calculations and the input file is available to any interested party. Send a 5.25 inch (1.2 MB) or 3.5 inch (1.44 MB) formatted diskette to the authors with request.
[26]E. Hecht and A. Zajac, *Optics* (Addison-Wesley, Menlo Park, 1974), p 305.
[27]Born and Wolf, Ref. 20, pp. 327–328.
[28]Reference 20, Chap. 13.
[29]In terms of the laboratory angle, $\Delta d = \lambda/2(n_2^2 - \sin^2\theta_1)^{1/2}$.